American Mineralogist, Volume 92, pages 1464–1473, 2007

Jarosite–hydronium jarosite solid-solution series with full iron site occupancy: Mineralogy and crystal chemistry

Laurel C. Basciano* and Ronald C. Peterson

Department of Geological Sciences and Geological Engineering, Queen's University, Kingston, Ontario, Canada

Abstract

Structural changes within the jarosite–hydronium jarosite solid-solution series, $(K,H_3O)Fe_3(SO_4)_2(OH)_6$, were investigated by X-ray Rietveld analysis of powder diffraction data collected from synthetic samples. All previous studies of jarosite solid solution consisted of samples that were non-stoichiometric with respect to iron. In this study, stoichiometric samples in the series were synthesized under hydrothermal conditions at 140 °C using starting materials of $Fe_2(SO_4)_3{\cdot}5H_2O + K_2SO_4 + H_2O$ in hydrothermal conditions. End-member potassium jarosite was also synthesized under similar conditions from a stoichiometric mixture of $FeCl_3 + KCl + LiCl + Fe(SO_4)_3{\cdot}5H_2O + H_2O$. Crystals were initially zoned with potassium-rich cores and hydronium-rich rims. Samples were homogenized by grinding and re-heating in the reactant solution. One iron deficient sample was synthesized to determine the effect of non-stoichiometry. Substitution of H_3O by K changes the unit-cell parameters in a linear fashion; *c* increases significantly and *a* decreases to a lesser degree. Unit-cell parameters from stoichiometric samples determined in this study are larger than synthetic samples analyzed in previous studies as a result of full iron occupancy. Potassium substitution in the alkali site (A site) mainly affects the A-O2 bond length, which causes the Fe-O2 and Fe-O3 bonds to lengthen and shorten, respectively. As potassium substitutes into the structure, there is an overall increase in the *c* axis. Iron deficiency leads to a significant decrease in unit-cell volume (large in *c*, minor in *a*), which is caused by bond length Fe-O3, which is markedly shorter than stoichiometric samples with similar potassium occupancy. The synthetic samples are compared with natural samples of jarosite and hydronium jarosite collected from mine waste deposits in Rio Tinto, Huelva, Spain. The natural samples have close to full iron occupancy, resulting from high iron content in solution and correlate well to the synthetic samples. Samples were also analyzed using short-wave infrared spectroscopy (SWIR). It was found that there is a subtle difference in spectra between end-members hydronium jarosite and potassium jarosite that can be tracked across the solid-solution series.

Keywords: jarosite–hydronium jarosite solid-solution series, crystal synthesis, IR spectroscopy, SWIR, crystal structure, XRD data, Rietveld refinement

Introduction

The jarosite group of minerals is part of the alunite supergroup, which consists of 40 mineral species that have the general formula $AB_3(TO_4)_2(OH)_6$. There is extensive solid solution in the A, B, and T sites within the alunite supergroup, where A is H_3O^+, Na^+, K^+, Rb^+, Ag^+, Tl^+, NH^{4+}, $½Ca^{2+}$, or $½Pb^{2+}$; B is Fe^{3+} or Al^{3+}; and TO_4 is SO_4^{2-}, PO_4^{3-}, or AsO_4^{3-} (Scott 1987; Stoffregen and Alpers 1987). The jarosite group is characterized by B = Fe^{3+} and T = S. Jarosite (A = potassium) and natrojarosite (A = sodium) are the most prevalent naturally occurring jarosite group minerals and hydronium jarosite is rare, though most jarosite group minerals contain some hydronium in the A site (Ripmeester et al. 1986; Drouet and Navrotsky 2003; Majzlan et al. 2004). Hydronium jarosite will only form from alkali-deficient solutions, as alkali-rich jarosite forms preferentially. For the sake of clarity, jarosite, sensu stricto, will be referred to as potassium jarosite throughout this paper.

The jarosite group of minerals has been extensively studied as a result of its importance as a by-product of the metal-processing industry as well as being very common in acid-mine waste. Minerals within the jarosite group are commonly found in acidic, high-sulfate environments associated with mine tailings. Metal-rich acidic sulfate containing waters originate from the oxidation of sulfide minerals, such as pyrite (FeS_2). This natural process is amplified by human activities relating to mining and mineral processing, which exposes these minerals to water and air. Oxidation of sulfide minerals leads to the formation of soluble and insoluble metal-bearing sulfates, hydroxysulfates, and hydrous oxides. The formation of these secondary phases typically leads to the generation of acidic solutions. The mineral group jarosite commonly forms after ferrous iron in the acidic sulfate waters oxidizes to ferric iron. As jarosite is a sink for iron, it is used in the zinc industry as a means of eliminating iron that is commonly present in Zn-Fe solution concentrates. Annually, 125 000 tons of jarosite containing 25–36 wt% Fe is produced

* E-mail: basciano@students.geol.queensu.ca

(Dutrizac and Jambor 2000).

Jarosite has been identified as a possible mineral on Mars (Klingelhöfer et al. 2004) based on Mössbauer spectra. Jarosite on Mars may form through similar processes as it does on Earth, such as oxidation of sulfide minerals (Burns 1987, 1988; Papike et al. 2006). Jarosite is a hydrous mineral with approximately 10 wt% H_2O in the form of OH^- groups. The presence of jarosite on Mars would be important mineralogical evidence for the existence of water on this planet at some time in its history.

Natural and synthetic jarosite group minerals commonly have significant quantities of hydronium in the alkali (A) site and minor to major deficiencies in the iron (B) site. Most jarosite group minerals synthesized in previous studies and many natural jarosite group minerals have B site occupancies as low as 86%. Studies that address the iron and/or aluminum deficiency are Hendricks (1937), Kubisz (1970), Ripmeester et al. (1986), Drouet and Navrotsky (2003), and Drouet et al. (2004). The iron non-stoichiometry and hydronium substitution has led to discrepancies in the literature about the unit-cell parameters of potassium jarosite. It is thought that charge neutrality for the iron deficient samples is maintained by protonation of the hydroxyl groups in the structure, creating water molecules (Ripmeester et al. 1986).

Ripmeester et al. (1986) confirmed the presence of hydronium ions in the alunite structure using NMR (nuclear magnetic resonance) and Wills and Harrison (1996) proposed a model for the H_3O group in hydronium jarosite based on neutron diffraction data. The structure of hydronium jarosite was refined by Majzlan et al. (2004) based on X-ray data. Several studies exist in the literature which address hydronium in the jarosite structure, including Drouet and Navrotsky (2003), Kubisz (1970), Dutrizac and Kaiman (1976), and Ripmeester et al. (1986).

Stoichiometric alunite group minerals have been synthesized previously by Rudolph et al. (2003). The potassium-hydronium alunite solid-solution series was synthesized under hydrothermal conditions, with stoichiometric end-members. These experiments were done at 180–200 °C, which is not possible for jarosite, as Fe_2O_3 and $Fe(OH)SO_4$ form above 160 °C (Kubisz 1970). Natrojarosite with full sodium occupancy was synthesized by a two-step method described by Stoffregen (1993). The method involved synthesizing non-stoichiometric natrojarosite with 67% alkali site occupancy and then heating the natrojarosite in a 1.0 *m* H_2SO_4-0.5Na_2SO_4 solution at 200 °C for 8 days, which yielded an A site occupancy of 98%.

The purpose of this work is to study the crystal chemical effect of hydronium substitution and iron deficiency on the crystal structure of potassium jarosite. The $(H_3O)_{1-x}K_xFe_3(SO_4)_2(OH)_6$ solid-solution series, with x = 0.0, 0.10, 0.20, 0.35, 0.51, 0.60, 0.70, 0.86, and 0.95, and full iron occupancy, has been synthesized by hydrothermal methods. Rietveld refinements of powder diffraction patterns show the structural changes caused by the replacement of K^+ by H_3O^+. In addition, structural changes as a result of the non-stoichiometry of Fe^{3+} are examined.

Natural samples in the hydronium–potassium jarosite solid-solution series were collected from mine waste associated with Rio Tinto mine and surrounding smaller mines in Huelva Province, SW Spain to study in conjunction with the synthetic samples. The Rio Tinto mining district is part of the Iberian Pyrite Belt (IPB). The area is underlain by the Lower Carboniferous Volcanic-Sedimentary Complex, which host massive and stock work pyrite ore bodies containing base and precious metals such as Cu, Pb, Zn, Au, and Ag. The IPB has been mined using both opencast and underground mining methods, from approximately 2500 BC to the present day (Hudson-Edwards et al. 1999). During this time approximately 300 million tons of ore have been extracted (García García 1996) producing extensive tailing deposits and other mining wastes, creating acid-mine waste rich alluvium in the Rio Tinto and Odiel rivers. One of the collected natural samples has close to full iron occupancy, which is probably due to the extremely high iron content of the acidic waters as well as slow equilibrium growth in a natural setting. In addition, the samples have low sodium content, making them ideal as natural representatives for the synthetic analogues grown in this study.

Short wave infrared (SWIR) spectra were collected from the synthetic samples to determine the changes due to H_3O content. SWIR is often used in the field to evaluate minerals associated with acid-mine waste. The method is based on detecting the presence of molecular water, OH, and other hydroxyl radicals in the mineral structure, which can be used for mineral identification. Hyperspectral imaging has also been used to identify alunite group minerals near mining sites, and to map acidic mine waste (Clark et al. 2003; King et al. 1995; Kruse et al. 1989; Swayze et al. 2000).

Experimental methods

Sample synthesis

The solid-solution series $(H_3O)_{1-x}K_xFe_3(SO_4)_3(OH)_6$ was synthesized hydrothermally in stainless steel vessels at 140 °C for 48 h. Synthesis conditions are summarized in Table 1. To precipitate sufficient sample for Rietveld analysis the volume of starting liquid was 100 mL. The sample container consisted of polypropylene bottles (125 mL), which were placed in stainless steel vessels. The vessels were fabricated from stainless steel threaded pipe and two lids. One lid is welded in place and the other is threaded. To ensure a tight seal, a silicone plug is used in the lid. The stainless steel vessels were partially filled with water. The pressure inside the vessels and polypropylene bottles was approximately the vapor pressure of water at 140 °C, 3.58 atm. Samples were synthesized by using a variation of the method described by Wills and Harrison (1996) for synthesizing hydronium jarosite. Forty grams of ACROS brand $Fe_2(SO_4)_3{\cdot}5H_2O$ and varying amounts of Fisher Scientific K_2SO_4 (0–2.0 g) were mixed with deionized water to a volume of 100 mL at room temperature. These conditions were used to ensure a high concentration of Fe^{3+} ions in solution. It was noted by Kubisz (1970) that low relative concentration of Fe^{3+} ions in the starting solutions resulted in deficiency of iron in synthesized jarosites. During the H_3O–K jarosite solid solution synthesis, potassium-rich jarosite precipitated out of solution first in all samples, followed by hydronium-rich jarosite. This was noted on preliminary XRD patterns and confirmed by SEM analysis. XRD scans showed several peaks that were broadened and, in some extreme cases split, forming two separate peaks. The peak broadening was most evident for peak (006) where there is a large difference in peak position between potassium-rich and potassium-poor phases in the mixture. To produce a single homogeneous phase, samples were finely ground in a McCrone Micronizing Mill after the initial synthesis and heated at 140 °C in the reactant solution. Samples were analyzed every 3 days using XRD to determine sample homogeneity. Samples with compositions close to hydronium jarosite were more difficult to homogenize and had to be exchanged for a longer period of time (sample B, 20 days; sample H, 3 days). The samples were deemed to be homogeneous when the 006 peak was sharp and the full width at half maximum (FWHM) did not decrease with further annealing. Figure 1 shows part of an XRD scan (peak 006) of sample B before exchange compared to hydronium jarosite and potassium jarosite to show the peak splitting/broadening.

End-member potassium jarosite could not be grown using the above method as hydronium remains in the structure with high initial potassium content in

TABLE 1. Synthesis conditions and chemical compositions of synthetic and natural jarosite samples

	Starting solution compositions (g)		Analytical results (ICP-OES) (% occupancy) and formula				
Synthetic samples	$K_2(SO_4)$	$Fe(SO_4)_3{\cdot}xH_2O$	Fe%	K%	Na%	S%	Formula
A	0.00	40	102.050	0.374	na	100	$(K_0H_3O_1)Fe_{3.06}(SO_4)_2(OH)_6$
B	0.08	40	102.818	10.156	na	100	$(K_{0.102}H_3O_{0.898})Fe_{3.08}(SO_4)_2(OH)_6$
C	0.16	40	103.554	19.973	na	100	$(K_{0.200}H_3O_{0.800})Fe_{3.11}(SO_4)_2(OH)_6$
D	0.24	40	97.686	34.976	na	100	$(K_{0.350}H_3O_{0.650})Fe_{2.93}(SO_4)_2(OH)_6$
E	0.50	40	98.085	51.291	na	100	$(K_{0.512}H_3O_{0.488})Fe_{2.94}(SO_4)_2(OH)_6$
F	1.00	40	97.405	60.506	na	100	$(K_{0.605}H_3O_{0.395})Fe_{2.92}(SO_4)_2(OH)_6$
G	1.50	40	100.546	70.367	na	100	$(K_{0.704}H_3O_{0.296})Fe_{3.02}(SO_4)_2(OH)_6$
H	2.00	40	98.830	85.693	na	100	$(K_{0.857}H_3O_{0.143})Fe_{2.96}(SO_4)_2(OH)_6$
I*	na	na	95.727	95.291	na	100	$(K_{0.953}H_3O_{0.047})Fe_{2.87}(SO_4)_2(OH)_6$
J†	12.50	5	86.345	87.321	na	100	$(K_{0.873}H_3O_{0.127})Fe_{2.59}(SO_4)_2(OH)_6$
Natural samples							
7-13-2-1	na	na	99.731	1.858	1.918	100	$(K_{0.019}H_3O_{0.981}Na_{0.019})Fe_{2.99}(SO_4)_2(OH)_6$
7-11-3-8	na	na	91.088	84.304	1.080	100	$(K_{0.843}H_3O_{0.146}Na_{0.011})Fe_{2.73}(SO_4)_2(OH)_6$

* Synthesized in chloride media similar to Frost et al. (2005), see text for details.
† Synthesized using method from Drouet and Navrotsky (2003), see text for details.

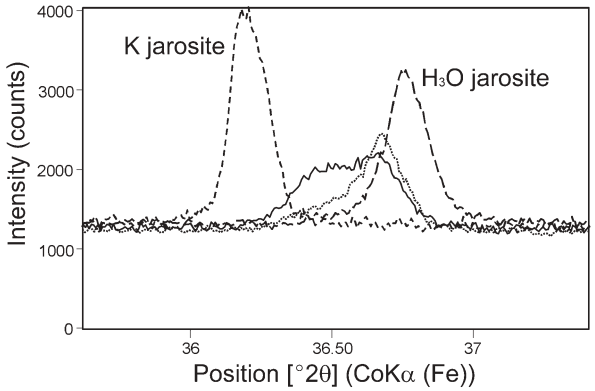

FIGURE 1. XRD plot showing the 006 peak from hydronium jarosite (long dashes, right), potassium jarosite (medium dashes, left), sample B before exchange (solid line) and sample B after exchange (dotted line). Sample B before exchange had not been ground and re-equilibrated with the reactant solution and shows peak splitting/broadening.

the starting solution. Close to fully occupied potassium jarosite was grown in a chloride-rich medium using a similar method to Frost et al. (2005). Five milliliters of 1.23 *M* $FeCl_3$ and 0.5 g KCl were dissolved in 12 mL concentrated LiCl solution. Six grams of $Fe(SO_4)_3{\cdot}5H_2O$ was dissolved in 25 mL deionized water and slowly added to the chloride solution. The final solution was heated for 48 h in a stainless steel pressure vessel at 140 °C. It was found that the high chloride concentration reduced the amount of hydronium entering the structure. This procedure yielded potassium jarosite with 95.3% K, as determined by inductively coupled plasma optical emission spectroscopy (ICP-OES). All samples were rinsed thoroughly with de-ionized water, filtered, and dried at 120 °C to eliminate any excess water. Drying at this temperature did not influence the X-ray diffraction pattern of the samples. All samples consisted of intergrown rhombohedral (pseudocubic) crystals ranging from <10 µm (initial growth adjacent to jar wall) to 100 µm (final growth). One sample was synthesized using a method similar to that of Drouet and Navrotsky (2003) to obtain a sample that is non-stoichiometric with respect to iron. This sample was used as a comparison to the rest of the solid-solution series grown during this study. The sample was precipitated from 5 g $Fe_2(SO_4)_3{\cdot}5H_2O$, 12.5 g K_2SO_4, and 250 mL deionized water, which was stirred for two hours at 95 °C .

X-ray diffraction and Rietveld refinement

Powder-diffraction data were collected from 15–100 °2θ (Fe filtered Co*K*α radiation) from a back-packed sample using a Panalytical X'Pert theta-theta diffractometer and an X'celerator position-sensitive detector equipped with incident- and diffracted-beam soller slits, and 1/2° divergence and 1° anti-scatter slits. The normal-focus Co X-ray tube was operated at 40 kV and 45 mA. Profiles were taken with a step interval of 0.008 2θ, counting time per step 30 s. To eliminate preferred orientation, samples were ground for 2 min in a McCrone Micronizing Mill, mixed with Fisher Scientific Al_2O_3 (ground for 5 min) and then backpacked on 320 grit sandpaper. The alumina is used to influence the packing geometry of the jarosite powder, helping to randomly orient the grains. Approximately 30% of the final sample is alumina. The structures were refined with the Rietveld refinement program Topas Academic (Coelho 2004). Starting atomic parameters were taken from Majzlan et al. (2004). The instrument parameters were modeled using a full axial divergence model defined by Cheary and Coelho (1998). Co*K*α source emission profiles were taken from Hölzer et al. (1997). Broadening due to crystallite size was refined using the Double-Voigt approach (Balzar 1999). The oxygen of the H_3O group was located at (0, 0, 0) similar to Majzlan et al. (2004). The model put forth by Wills and Harrison (1996), who moved the oxygen of the H_3O group to (0, 0, z) and invoked disorder at the hydronium site, was not followed. The occupancy of potassium in the A site was fixed to the occupancy determined with ICP-OES and the T site is assumed to be fully occupied by S. The refined occupancy of oxygen in the A site for the end-member hydronium jarosite was found to 0.92(1), which is similar to results of Majzlan et al. (2004) (discussed below). Based on the hydronium jarosite results, the occupancy of the hydronium in the A site was refined independently for samples containing potassium. For samples A and B the occupancy K + H_3O was less than 1, with the combined occupancy increasing with increasing potassium content. The occupancy of A site was refined to 1.02 for sample C, which is within 1 e.s.d. of 1.The alkali site occupancy for the samples in the remaining solid-solution series was constrained so that K + H_3O = 1. When the occupancy of the site was not restrained in these samples many of the refinements became unstable, with the occupancy of the alkali site exceeding 1 and bond lengths becoming unreasonable. Starting hydrogen positions (OH group) were taken from the single-crystal study of hydronium jarosite by Majzlan et al. (2004). Without a restraint the O3-H bond length was significantly shorter than typical values. As hydrogen is not easily detected by X-rays, the positions are not as accurate as heavier atoms. The O-H bond length was restrained at 0.8 Å instead of 0.98 Å, which is the average O-H bond length in crystalline solids refined by X-ray diffraction (Baur 1972), because observed O-H distances in X-ray determinations tend to be on average 0.2 Å shorter than in neutron diffraction (Baur 1972). The displacement parameters of the H atoms were fixed at 2 and not refined. Rietveld quality data were also collected and analyzed for two natural samples from Rio Tinto, Spain. The samples consisted of jarosite and quartz. Both phases were included in the refinement. No alumina was added to these samples and they were ground using a mortar and pestle. The refinements were done in the same manner as the synthetic samples. Details of data collection and structure refinement are given in Table 2. A final plot of observed and calculated intensities for a representative Rietveld refinement is shown in Figure 2.

Short-wave infrared reflectance spectroscopy (SWIR)

Short-wave infrared reflectance spectra of the synthetic K–H_3O jarosite solid-solution series were collected using a Portable Infrared Mineral Analyzer, Integrated Spectronics PIMA SP instrument, which measures in the 1200–2600 nm range. The samples were analyzed as finely ground dry powders.

Chemical analysis

The iron, potassium, and sulfur content of the solid jarosite samples and reactant solutions were determined using a Varian vista CCD Simultaneous ICP-OES at Analytical Services Unit, Queen's University. The solid samples were digested in aqua regia and both the digested samples and reactant solutions were diluted for

TABLE 2. Data collection and structure refinement details: hydronium jarosite–jarosite $R\bar{3}m$

	A	B	C	D	E	F	G	H	I	J	7-13-2-1	7-11-3-8
x	0.00	0.10	0.20	0.35	0.51	0.60	0.70	0.86	0.95	0.87	0.02	0.84
a (Å)	7.3552(2)	7.3521(1)	7.3428(2)	7.3373(1)	7.33009(8)	7.32070(6)	7.3112(1)	7.3070(1)	7.30293(8)	7.3063(1)	7.3478(1)	7.3128(1)
c (Å)	16.9945(4)	17.0108(3)	17.0316(5)	17.1030(3)	17.1374(2)	17.1517(3)	17.1792(2)	17.1916(3)	17.2043(2)	17.0341(4)	17.0280(2)	17.1973(4)
V (Å)	796.21(4)	796.31(3)	795.26(5)	797.40(3)	797.43(2)	796.05(2)	795.27(3)	794.93(3)	794.62(2)	787.50(3)	796.18(2)	796.44(3)
R_p	3.571	4.236	5.321	3.408	2.903	4.111	3.378	3.668	3.289	4.137	3.013	3.589
R_{wp}	4.773	5.849	8.020	5.052	3.994	5.707	4.415	4.788	4.288	5.441	3.976	4.988
R_{exp}	3.882	3.923	4.098	2.726	2.787	3.513	3.621	4.204	3.570	4.479	3.078	3.467
S	1.230	1.491	1.957	1.854	1.433	1.624	1.219	1.139	1.201	1.215	1.291	1.439
D-W	0.691	0.498	0.300	0.336	0.567	0.483	0.726	0.825	0.745	0.731	0.645	0.523

Notes: Step interval (°2θ) 15–100°, step 0.008. R_p = *R*-pattern, R_{wp} = weighted-pattern, R_{exp} = *R*-expected, S (R_{wp}/R_{exp}) = Goodness of fit (Young 1993). D-W = Durbin-Watson *d*-statistic (Hill and Flack 1987).

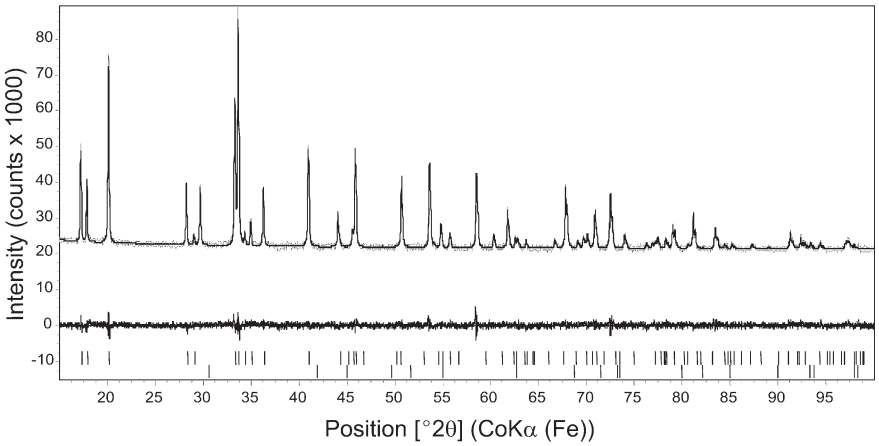

FIGURE 2. Rietveld refinement plot of sample D, $(K_{0.350}H_3O_{0.650})Fe_{2.93}(SO_4)_2(OH)_6$. The sample was refined with two phases (jarosite + alumina). The gray line is the observed data and the solid line is the calculated pattern. The vertical bars mark all possible Bragg reflections (Co$K\alpha_1$ and $K\alpha_2$), where upper and lower bar marks are jarosite and alumina, respectively. The difference between the observed and calculated patterns is shown at the bottom.

analysis. The average analytical error for each element is: Fe ±1%, K ±5%, and S ±2%. From these data the stoichiometry of the alkali and iron sites were determined in the solid samples based on the ratio of alkali and iron to sulfur. The percent of potassium and iron in these sites were normalized to 2 S per chemical formula based on the ideal chemical formula. The mol% potassium and iron in the reactant solutions were also normalized to sulfur for the sake of comparison. The chemical compositions of synthetic and natural samples are given in Table 1 and chemical compositions of the reactant solutions are shown in Figure 3.

Natural samples

Hydronium–potassium jarosite samples were collected in the current study from mine waste in the immediate vicinity of abandoned mines in the Rio Tinto mining area and alluvium along the Rio Tinto River. Only two samples were analyzed by Rietveld methods as most of the samples were mixed with several other minerals. The two samples analyzed were mixed only with quartz. Potassium-rich jarosite was collected from a small creek at the base of a tailings impoundment associated with Rio Tinto Mine (GPS coordinates: N 37°44'14.6" W 6°36'44.2"). The tailings consisted predominantly of sulfides, quartz and clay minerals. A sample of hydronium jarosite was collected from the bank of the Rio Tinto River, approximately 16 km from the mine, south of Berrocal where highway HV5137 crosses the river. The samples were very fine-grained yellow powders, which were washed in de-ionized water, filtered, and air dried before X-ray analysis.

RESULTS AND DISCUSSION

Synthesis experiments

As noted previously, potassium-rich jarosite precipitated out of solution first, followed by hydronium-rich jarosite. Even when a very low amount of potassium is added to the solution, the first jarosite precipitate has a very high potassium content. Sample D was examined before exchange using XRD and SEM analysis. After exchange, the split (006) peaks merge and move to higher 2θ (higher hydronium content) (Fig. 1). The jarosite precipitate forms a crust on the polypropylene jar walls, which was cross-sectioned and analyzed with a SEM to confirm that potassium-rich jarosite was precipitating out of solution first. As can be seen in Figure 4 the jarosite that precipitates out of solution first, closer to the polypropylene jar, is much higher in potassium than the jarosite in contact with the solution.

Figure 3 shows the partitioning of potassium and iron between the solution and precipitated crystals. As noted in previous studies (Brophy and Sheridan 1965; Brown 1970; Dutrizac 1983), potassium is preferentially taken into the jarosite structure over sodium and hydronium. Potassium jarosite is more thermodynamically stable than both sodium jarosite and hydronium jarosite (Drouet and Navrotsky 2003). The same results were also found in this study for potassium and hydronium. Nearly all the potassium that is added to the system is taken up in the jarosite crystals. Only in samples where the iron has become depleted, and therefore jarosite no longer precipitates, will appreciable amounts of potassium remain in solution (when K >> Fe in the starting solution). The iron in the precipitate remains relatively constant at 100% occupancy for all of the samples except for sample J. When the system is saturated with iron, the precipitating jarosite will have full iron occupancy. In sample J there was less iron in the starting solution; jarosite still precipitated but iron occupancy was less than one. As expected, the iron remaining in the reactant solution reduces as larger amounts of potassium are added. This trend is associated with yield volume of the samples. As the potassium in the reactant solution increases the jarosite yield increases dramatically, therefore reducing the amount of iron remaining in solution. The increase in yield correlating with

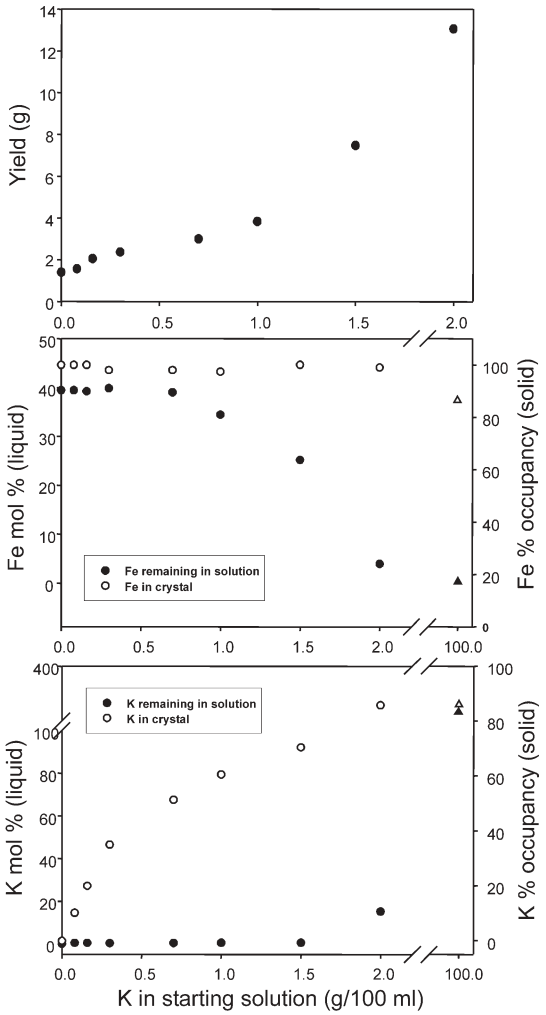

FIGURE 3. Yield and partitioning of potassium and iron between the solution and precipitated crystals as a function of K in the starting solution. Hydronium-rich jarosite is plotted on the left and potassium-rich jarosite is plotted on the right. The triangles in the lower two plots represent sample J, which was grown with significantly more potassium in the starting solution than the rest of the solid-solution series, resulting in lower iron occupancy. The potassium and iron in the solution and precipitating crystals were normalized to sulfur for the sake of comparison.

potassium content of the starting solution has also been discussed by Dutrizac (1983).

Relationship between structural parameters and potassium content

The XRD patterns of the $(H_3O)_{1-x}K_xFe_3(SO_4)_3(OH)_6$ solid-solution series show a progressive change in unit-cell parameters as a result of hydronium substitution. As determined by Rietveld refinement and ICP-OES all samples have close to full or full iron occupancy and the end-member potassium jarosite has 95.3% potassium occupancy. The reliability factors, positional parameters, site occupancies, and selected interatomic distances and angles obtained are given in Tables 2, 3, and 4.

A structural drawing of potassium jarosite is shown in Figure 5. The jarosite group crystallizes in space group $R\bar{3}m$ with Z = 3 (in the hexagonal unit cell). The basic structure of the jarosite group consists of SO_4 tetrahedra and Fe-cation octahedra, where the octahedra corner-share to form sheets perpendicular to the **c** axis. The SO_4 tetrahedra occur as two crystallographically independent sites within a layer; one set of SO_4 points toward +**c**, which alternate with another set pointing toward –**c**. The oxygen and hydroxyl group form an icosahedron, in which the alkali cation or hydronium group is located. The univalent cations (K^+, H_3O^+, Na^+, etc.) are surrounded by twelve anions, consisting of six oxygen atoms (O2), and six OH groups (O3).

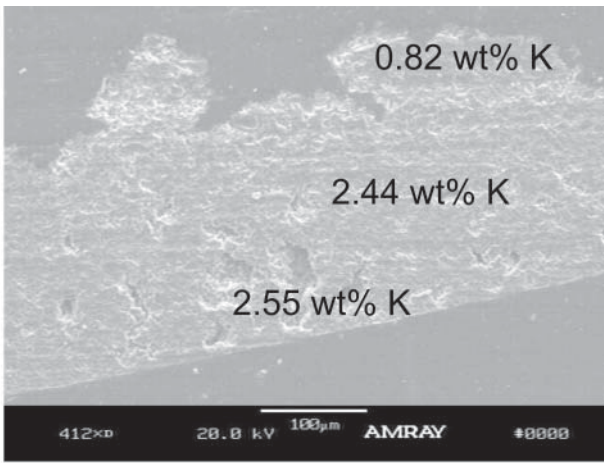

FIGURE 4. Secondary electron micrograph showing a cross section through synthetic jarosite. The bottom of the cross section was the first to grow and was found adhered to the bottle wall. The top of the section was the last to grow and was in contact with the reactant solution. Potassium was preferentially taken into the earlier jarosite crystals.

The unit-cell parameters a vs. c from the current study and previously synthesized members of the hydronium–potassium jarosite solid-solution series are plotted in Figure 6. Natural samples from previous studies are not included as many contain sodium as well, or chemical data are not available. The data from this study fall close to a straight line (correlation coefficient r^2 = 0.97) connecting hydronium jarosite and potassium jarosite, therefore following Vegard's Law, confirming ideal solid solution. Unit-cell parameters vs. potassium content for synthetic samples from the current study are given in Figure 7. Substitution of H_3O by K increases unit-cell parameter c significantly and decreases a to a lesser degree. All data points for a and c fall close to a straight line; correlation coefficients for a are r^2 = 0.98 and c are r^2 = 0.96. All the jarosite samples from this study, which have full iron occupancy, have larger unit-cell parameters than most of the samples grown in previous studies. Jarosite group minerals grown in previous studies are non-stoichiometric with respect to iron, which reduces the unit-cell parameters and causes the scatter of data points.

Polyhedra bond lengths A-O2, O3, Fe-O2, and O3 are shown in Figures 8 and 9. With increasing K substitution bond lengths A-O3 remain approximately the same and A-O2 decreases. An ideal hydronium ion has on average O-H bond length of ~0.98 Å and H-O-H bond angle of ~111° (Begemann and Saykally 1985). Chiari and Ferraris (1982) show that the minimum, maximum

TABLE 3. Refined atomic positions, displacement parameters and occupancies of synthetic and natural jarosite samples

Site	W	*x*	*y*	*z*	*B*	occ
Sample A, K occ = 0						
H_3O	3*a*	0	0	0	3.4(5)	0.92(1)
Fe	9*d*	0.166667	–0.166667	–0.16667	1.99(8)	1
S	6*c*	0	0	0.3095(2)	0.9(1)	1
O1	6*c*	0	0	0.3946(3)	2.6(3)	1
O2	18*h*	0.2253(3)	–0.2253(3)	–0.0565(2)	1.5(2)	1
O3	18*h*	0.1279(2)	–0.1279(2)	0.1368(1)	0.5(1)	1
H	18*h*	0.163(1)	–0.163(1)	0.100(1)	2	1
Sample B, K occ = 0.10						
K	3*a*	0	0	0	4.1(6)	0.10
H_3O	3*a*	0	0	0	4.1(6)	0.86(1)
Fe	9*d*	0.166667	–0.166667	–0.16667	2.55(8)	1
S	6*c*	0	0	0.3098(2)	2.0(1)	1
O1	6*c*	0	0	0.3955(4)	7.0(4)	1
O2	18*h*	0.2255(3)	–0.2255(3)	–0.0574(2)	2.5(2)	1
O3	18*h*	0.1265(2)	–0.1265(2)	0.1350(2)	0.19(1)	1
H	18*h*	0.186(2)	–0.186(2)	0.125(1)	2	1
Sample C, K occ = 0.20						
K	3*a*	0	0	0	2.8(6)	0.20
H_3O	3*a*	0	0	0	2.8(6)	0.81(2)
Fe	9*d*	0.166667	–0.166667	–0.16667	3.0(1)	1
S	6*c*	0	0	0.3109(2)	2.2(2)	1
O1	6*c*	0	0	0.3962(3)	6.3(5)	1
O2	18*h*	0.2264(3)	–0.2264(3)	–0.0589(3)	2.4(2)	1
O3	18*h*	0.1309(3)	–0.1309(3)	0.1334(2)	1.9(2)	1
H	18*h*	0.155(2)	–0.155(2)	0.092(1)	2	1
Sample D, K occ = 0.35						
K	3*a*	0	0	0	1.4(2)	0.35
H_3O	3*a*	0	0	0	1.4(2)	0.65
Fe	9*d*	0.166667	–0.166667	–0.16667	2.48(7)	1
S	6*c*	0	0	0.3100(1)	1.27(9)	1
O1	6*c*	0	0	0.3961(2)	3.8(2)	1
O2	18*h*	0.2242(2)	–0.2242(2)	–0.0569(2)	2.3(1)	1
O3	18*h*	0.1284(2)	–0.1284(2)	0.1365(1)	1.2(1)	1
H	18*h*	0.160(1)	–0.160(1)	0.097(1)	2	1
Sample E, K occ = 0.51						
K	3*a*	0	0	0	1.1(1)	0.51
H_3O	3*a*	0	0	0	1.1(1)	0.49
Fe	9*d*	0.166667	–0.166667	–0.16667	1.98(5)	1
S	6*c*	0	0	0.3089(1)	1.39(7)	1
O1	6*c*	0	0	0.3940(3)	3.2(2)	1
O2	18*h*	0.2224(2)	–0.2224(2)	–0.0557(1)	2.5(1)	1
O3	18*h*	0.1266(1)	–0.1266(1)	0.1358(1)	0.93(9)	1
H	18*h*	0.177(1)	–0.177(1)	0.1105(8)	2	1
Sample F, K occ = 0.60						
K	3*a*	0	0	0	1.1(2)	0.60
H_3O	3*a*	0	0	0	1.1(2)	0.40
Fe	9*d*	0.166667	–0.166667	–0.16667	2.3(1)	1
S	6*c*	0	0	0.3096(3)	1.9(2)	1
O1	6*c*	0	0	0.3953(5)	4.6(4)	1
O2	18*h*	0.2213(3)	–0.2213(3)	–0.0556(3)	2.7(2)	1
O3	18*h*	0.1270(2)	–0.1270(2)	0.1360(2)	2.0(2)	1
H	18*h*	0.177(2)	–0.177(2)	0.111(1)	2	1
Sample G, K occ = 0.70						
K	3*a*	0	0	0	0.3(1)	0.70
H_3O	3*a*	0	0	0	0.3(1)	0.30
Fe	9*d*	0.166667	–0.166667	–0.16667	1.26(6)	1
S	6*c*	0	0	0.3092(2)	1.2(1)	1
O1	6*c*	0	0	0.3958(3)	2.3(2)	1
O2	18*h*	0.2213(2)	–0.2213(2)	–0.0553(2)	2.5(2)	1
O3	18*h*	0.1267(1)	–0.1267(1)	0.1350(1)	0.4(1)	1
H	18*h*	0.173(1)	–0.173(1)	0.107(1)	2	1
Sample H, K occ = 0.86						
K	3*a*	0	0	0	1.4(1)	0.86
H_3O	3*a*	0	0	0	1.4(1)	0.14
Fe	9*d*	0.166667	–0.166667	–0.16667	1.3(1)	1
S	6*c*	0	0	0.3082(2)	1.8(1)	1
O1	6*c*	0	0	0.3953(2)	3.9(2)	1
O2	18*h*	0.2214(2)	–0.2214(2)	–0.0549(1)	2.1(1)	1
O3	18*h*	0.1254(1)	–0.1254(1)	0.1350(1)	0.7(1)	1
H	18*h*	0.185(1)	–0.185(1)	0.125(1)	2	1
Sample I, K occ = 0.95						
K	3*a*	0	0	0	1.04(8)	0.95
H_3O	3*a*	0	0	0	1.04(8)	0.05
Fe	9*d*	0.166667	–0.166667	–0.16667	1.8(5)	1
S	6*c*	0	0	0.3088(1)	1.15(7)	1
O1	6*c*	0	0	0.3939(2)	1.8(2)	1
O2	18*h*	0.2211(1)	–0.2211(1)	–0.0544(1)	1.52(9)	1
O3	18*h*	0.1252(1)	–0.1252(1)	0.1344(1)	0.80(8)	1
H	18*h*	0.1863(9)	–0.1863(9)	0.1289(8)	2	1
Sample J, K occ = 0.87, Fe occ = 0.86						
K	3*a*	0	0	0	2.4(2)	0.87
H_3O	3*a*	0	0	0	2.4(2)	0.13
Fe	9*d*	0.166667	–0.166667	–0.16667	2.7(1)	0.86
S	6*c*	0	0	0.3111(3)	1.7(2)	1
O1	6*c*	0	0	0.3966(5)	3.5(4)	1
O2	18*h*	0.2227(4)	–0.2227(4)	–0.0568(4)	2.5(2)	1
O3	18*h*	0.1278(2)	–0.1278(2)	0.1360(2)	2.1(2)	1
H	18*h*	0.168(2)	–0.168(2)	0.102(2)	2	1
Sample 7-13-2-1, K occ = 0.02, Fe occ = 1						
K	3*a*	0	0	0	1.4(4)	0
H_3O	3*a*	0	0	0	1.4(4)	1
Fe	9*d*	0.166667	–0.166667	–0.16667	1.95(7)	1
S	6*c*	0	0	0.3095(2)	1.1(1)	1
O1	6*c*	0	0	0.3949(3)	2.6(2)	1
O2	18*h*	0.2243(3)	–0.2243(3)	–0.0566(2)	2.2(1)	1
O3	18*h*	0.1267(1)	–0.1267(1)	0.1356(1)	0.9(1)	1
H	18*h*	0.165(1)	–0.165(1)	0.1000(8)	2	1
Sample 7-11-3-8, K occ = 0.84, Fe occ = 0.91						
K	3*a*	0	0	0	1.4(1)	0.84
H_3O	3*a*	0	0	0	1.4(1)	0.16
Fe	9*d*	0.166667	–0.166667	–0.16667	1.62(7)	0.91
S	6*c*	0	0	0.3090(2)	1.5(1)	1
O1	6*c*	0	0	0.3935(4)	1.4(2)	1
O2	18*h*	0.2215(2)	–0.2215(2)	–0.0565(2)	2.8(2)	1
O3	18*h*	0.1274(2)	–0.1274(2)	0.1367(2)	1.0(1)	1
H	18*h*	0.166(1)	–0.166(1)	0.102(1)	2	1

Note: Numbers in parentheses in this and subsequent tables are estimated standard deviations.

and average O–H···O bond distances are 2.617, 3.085, and 2.835 Å, respectively, for water molecules in crystalline substances. Since the position of H was not determined for the H_3O^+, possible orientations for the H_3O group in the A polyhedra are based on hydronium geometry and bond length trends through the solid-solution series. The oxygen of the hydronium group is located in the center of the polyhedra, and it is likely that the hydrogen atoms are hydrogen bonded to the O2 atoms located roughly around the horizontal of the A polyhedra (Fig. 10). There are six O2 atoms in the polyhedra, three slightly above the horizontal and three slightly below (Fig. 5). The average bond angle between O2 atoms and the A site in hydronium jarosite is 110.4°and the bond distance between the A site and the O2 atoms is 3.026 Å. This angle is ideal for hydronium geometry and the bond length is within the range of O-H···O distances commonly found for water molecules in crystalline substances (Begemann and Saykally 1985; Chiari and Ferraris 1982). Another possible orientation of the hydronium group was proposed by Grohol et al. (2003) and Kubisz (1970), in which the protons from H_3O^+ in the A site transfer to neighboring OH^- (O3) forming H_2O. This is based on infrared data and ^2H NMR spectroscopy showing evidence of H_3O^+, H_2O, and OH^- in hydronium jarosite. The average bond angle between O3 atoms and the A site in hydronium jarosite is 59.6°, which is significantly smaller than the average hydronium bond angle of ~111°. Based solely on bond angles between O2 and O3 atoms, this scenario is not as likely as the hydronium group hydrogen bonding to the O2 atoms. As the A site in hydronium jarosite is not fully occupied with hydronium

TABLE 4. Selected interatomic distances (Å) and angles (°)

	A	B	C	D	E	F	G	H	I	J	7-13-2-1	7-11-3-8
K occ	0.000	0.102	0.200	0.350	0.512	0.605	0.704	0.857	0.953	0.873	0.011	0.843
K,H_3O-O3 ×6	2.839(2)	2.806(3)	2.817(4)	2.848(2)	2.829(2)	2.835(3)	2.821(2)	2.811(2)	2.802(2)	2.826(4)	2.817(2)	2.832(3)
K,H_3O-O2 ×6	3.026(4)	3.033(3)	3.049(4)	3.010(3)	2.981(2)	2.964(4)	2.959(3)	2.957(2)	2.949(2)	2.980(5)	3.013(3)	2.972(3)
Average	2.9325	2.9195	2.933	2.929	2.905	2.8995	2.89	2.884	2.8755	2.903	2.915	2.902
Fe-O3 ×4	1.9904(9)	1.992(1)	1.986(5)	1.9898(9)	1.9847(7)	1.983(1)	1.9845(9)	1.9794(8)	1.9806(7)	1.982(1)	1.9899(7)	1.985(1)
Fe-O2 ×2	2.015(4)	2.005(3)	2.014(2)	2.014(3)	2.029(2)	2.027(5)	2.034(3)	2.042(3)	2.050(2)	2.002(6)	2.012(3)	2.011(3)
Average	1.999	1.996	1.995	1.998	1.999	1.998	2.001	2.000	2.004	1.989	1.997	1.994
S-O1	1.447(7)	1.459(7)	1.453(7)	1.474(4)	1.458(5)	1.470(9)	1.487(7)	1.497(6)	1.463(5)	1.456(9)	1.455(6)	1.437(6)
S-O2 ×3	1.485(4)	1.489(3)	1.496(5)	1.501(3)	1.507(2)	1.522(4)	1.517(3)	1.507(3)	1.510(2)	1.518(5)	1.496(3)	1.525(3)
Average	1.476	1.482	1.485	1.494	1.495	1.509	1.510	1.505	1.498	1.503	1.486	1.503
O2-Fe-O3 ×4	89.6(1)	89.8(1)	89.13(8)	89.8(8)	88.92(7)	88.7(1)	88.08(9)	88.08(9)	87.65(7)	89.2(1)	89.61(9)	88.48(9)
O2-Fe-O3 ×4	90.4(1)	90.2(1)	90.87(8)	90.3(8)	91.08(7)	91.3(1)	91.92(9)	91.92(9)	92.35(7)	90.8(1)	90.39(9)	91.52(9)
O3-Fe-O3 ×2	89.7(1)	88.9(1)	88.59(2)	89.5(1)	89.06(9)	89.4(1)	88.9(1)	87.98(9)	87.67(8)	90.0(2)	89.18(9)	89.4(1)
O3-Fe-O3 ×2	90.3(1)	91.1(1)	91.41(2)	90.5(1)	90.95(9)	90.7(2)	91.1(1)	92.02(9)	92.33(8)	90.0(2)	90.82(9)	90.6(1)
O1-S-O2 ×3	112.0(1)	112.7(4)	114.6(1)	112.47(8)	110.86(9)	111.07(4)	110.7(1)	109.9(1)	109.93(8)	112.8(2)	111.90(9)	111.85(4)
O2-S-O2 ×3	106.9(2)	106.0(1)	103.9(3)	106.3(2)	108.1(1)	107.8(2)	108.2(2)	109.0(2)	109.01(8)	105.9(3)	106.9(2)	107.0(1)
Average	109.5	109.4	109.3	109.4	109.5	109.4	109.5	109.5	109.5	109.4	109.4	109.4
O3-H	0.767(2)	0.77(2)	0.77(2)	0.780(2)	0.773(2)	0.775(3)	0.762(2)	0.774(2)	0.779(1)	0.77(3)	0.774(2)	0.793(2)
O3-H···O1	2.914(3)	2.910(3)	2.841(4)	2.893(1)	2.924(2)	2.909(4)	2.898(2)	2.915(2)	2.923(2)	2.881(3)	2.916(2)	2.918(4)

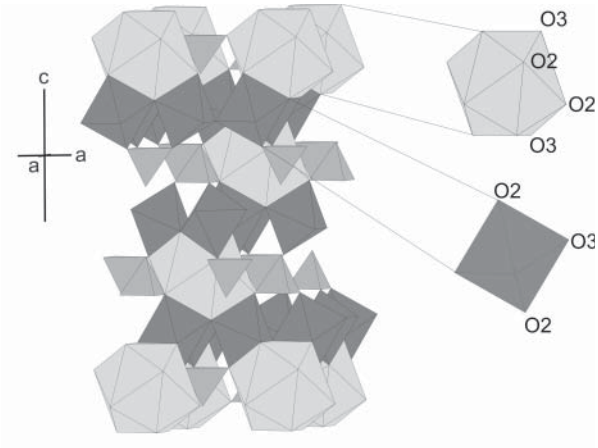

FIGURE 5. Polyhedral representation of the jarosite structure. Potassium polyhedra are light gray, iron octahedra are dark gray, and sulfate tetrahedra are mid-range gray.

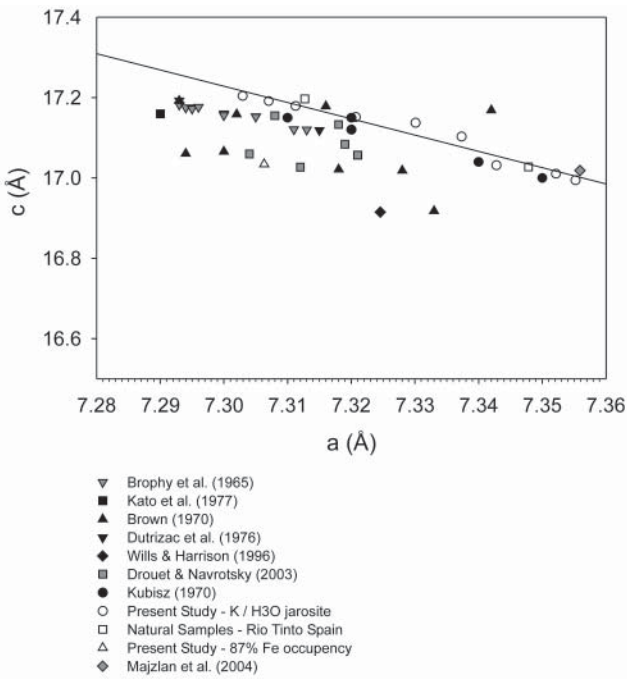

FIGURE 6. Unit-cell parameters *c* vs. *a* of synthetic samples containing only K and H_3O in the A site. All samples from the current synthetic study are shown as white circles. Note that the unit-cell dimensions fall close to a straight line, and are larger than most of the previous studies as they have full iron occupancy in the B site.

(found to be 92% occupied in the current study and 91% occupied by Majzlan et al. 2004), it is probable that charge neutrality is maintained by protonation of OH^- to form H_2O (Majzlan et al. 2004). This protonation would give evidence of H_3O^+, H_2O, and OH^- in spectroscopic studies of hydronium jarosite, as seen by Grohol et al. (2003) and Kubisz (1970).

It is commonly thought that the hydronium ion is disordered with two orientations with equal probability (Fig. 10). The A polyhedra are face sharing with the iron octahedra, which are corner sharing with sulfate tetrahedra. Additionally, O3 is a hydroxyl group, which is hydrogen bonded to O1 of the sulfate group. This bonding environment reduces the amount that the A-O3 bond length can change with substitutions in the A site. Therefore substitution in the A site mainly effects the A-O2 distances. As a result of the A-O2 bond shortening with K substitution, the Fe-O2 and Fe-O3 bonds lengthen and shorten, respectively. At low potassium content the A polyhedra are distorted and become more regular at higher potassium contents, though still distorted. In contrast, the iron (B) octahedra are increasingly distorted at higher potassium content and are very regular at low potassium concentration. As potassium substitutes into the structure, the distance between the A site and B site increases, therefore causing an increase in the length of the **c** axis.

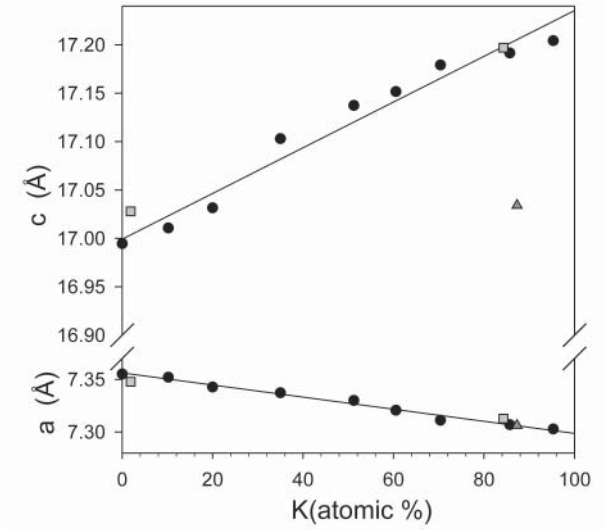

FIGURE 7. Unit-cell dimensions *a* and *c* vs. potassium occupancy in the alkali site. Black circles are from samples that are fully stoichiometric with respect to iron, the gray triangle is sample J, with 86.34% Fe occupancy, and the gray squares are natural samples 7-13-2-1 and 7-11-3-8, collected from Rio Tinto Mines, Spain. Error bars are smaller than the symbols.

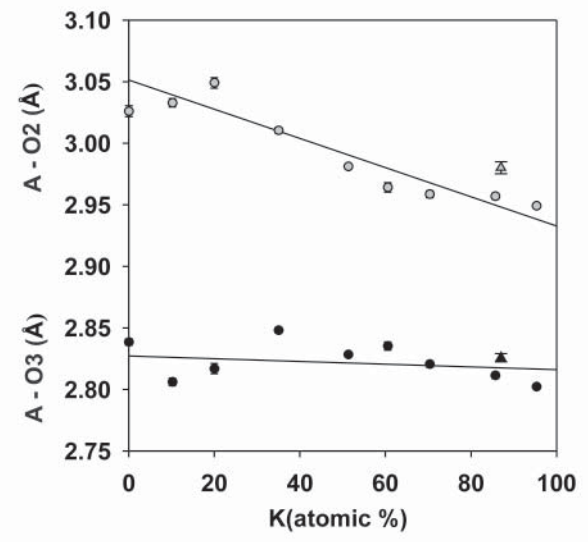

FIGURE 8. A-O polyhedra bond lengths vs. potassium occupancy in the alkali (A) site. Samples that are fully stoichiometric with respect to iron are represented by black and gray circles, and sample J (86.34% Fe occupancy) is represented by black and gray triangles.

Non-stoichiometry of the A and B sites

One sample was grown that was not fully stoichiometric with respect to iron. Sample J, which has 86.3% iron and 87.3% potassium occupancy (as determined by ICP-OES), has significantly different unit-cell parameters than the fully stoichiometric sample with similar potassium occupancy (sample H, 85.7% K). Unit-cell parameter *a* is very similar for both samples J and H. Unit-cell parameter *a* for sample J falls very close to the regression line for the stoichiometric solid-solution series. However, unit-cell parameter *c* is 0.16 Å smaller for sample J than for sample H and falls far below the regression line (Fig. 7). The Fe-O3 bond length is the same as stoichiometric samples but the Fe-O2 bond length is markedly shorter than in sample H, which has similar potassium occupancy. The Fe-O2 and O3 bond lengths of sample H are 2.042(3) and 1.9794(8) Å, respectively, and the average bond lengths of sample J are 2.002(6) and 1.982(1) Å, respectively. Correspondingly, the A-O2 bond length for sample J is longer than that for sample H.

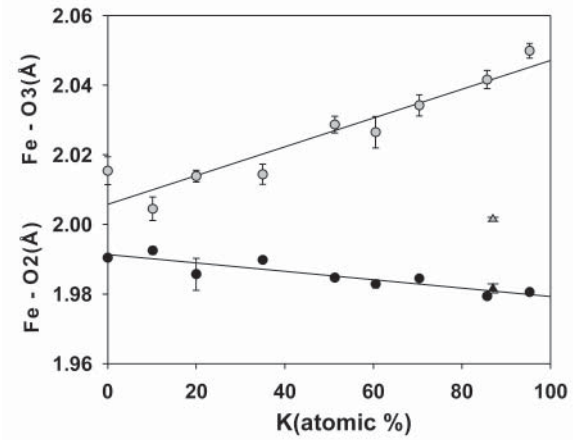

FIGURE 9. Fe-O octahedral bond lengths vs. potassium occupancy in the alkali site. Samples that are close to fully stoichiometric with respect to are iron are represented by black and gray circles, and sample J (86.34% Fe occupancy) is represented by black and gray triangles.

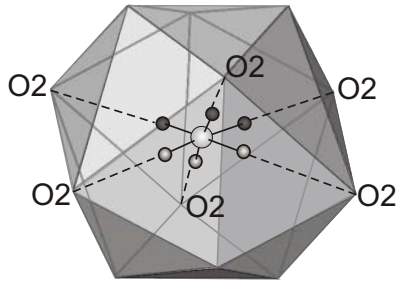

FIGURE 10. Hydronium polyhedra showing possible orientations of H_3O^+. The hydrogen are thought to be disordered and the two orientations of the hydronium group are shown. The oxygen is represented by white and the hydronium group can be pointed upward (dark gray H) or downward (mid-gray H). Hydrogen bonding to O2 atoms is represented by dashed lines.

Samples A and B are non-stoichiometric with respect to the alkali site, with the occupancy of K + H_3O < 1. This was only found in samples with very high hydronium content. This is similar to results found by Majzlan et al. (2004) for end-member hydronium jarosite. The A-O2 bond length is smaller than expected in sample A (hydronium jarosite) and B as a result of the lower occupancy, while A-O3 bond length is unaffected. As bond length A-O2 is smaller, Fe-O2 is longer by approximately the same amount (Table 4).

When the B site is not fully occupied by Fe^{3+}, it is thought

that charge neutrality is maintained by protonation of OH^- to form H_2O (Kubisz 1970; Wills and Harrison 1996). Majzlan et al. (2004) state that charge neutrality could be maintained in similar manner for partial occupancy of hydronium giving a general formula for the hydronium jarosite synthesized in this study $(H_3O_{0.92})Fe_3(SO_4)_2[(OH)_{5.92}(H_2O)_{0.16}]$. From Rietveld refinement, it appears that the A site is fully occupied with hydronium and potassium at higher potassium contents, but not for samples with lower potassium content.

Crystal chemistry of natural samples

The two natural samples from Rio Tinto, Spain (7-13-2-1 and 7-11-3-8) are close to fully occupied with respect to iron. Sample 7-13-2-1 has 1.9% K and 1.9% Na occupancy and therefore, can be described as a hydronium jarosite. Sample 7-11-3-8 is closer to stoichiometric (potassium) jarosite with 84.3% K and 1.1% Na occupancy. Both natural jarosite samples are structurally very close to the synthetic jarosite samples grown with full iron occupancy. ICP-OES results confirm that the samples do have close to full iron occupancy as well. The unit-cell parameters and bond lengths of the natural samples are plotted with the synthetic samples in Figures 6 and 7.

Waters associated with Rio Tinto are characterized by low pH values (1.5–2.7) and extremely high metal and sulfate concentrations (Hudson-Edwards et al. 1999). As determined by Hudson-Edwards et al. (1999), the concentration of iron is very high in the Rio Tinto River downstream of the mining area and decreases sharply near the estuary. Iron concentrations can be as high as 28 989 mg/L (Fernández-Remolar et al. 2005) and range from 2000–4300 mg/L before the estuary. Potassium-rich jarosite formed when there was potassium available (from the dissolution of feldspar and clay minerals), which is similar to results found in the current synthetic studies. Further downstream the Rio Tinto River hydronium jarosite forms, as all potassium has been removed from solution by jarosite (and other associated minerals) precipitating closer to the mining areas.

A natural jarosite sample structurally analyzed by Kato and Miuri (1977) has very similar unit-cell parameters and bond lengths as the end-member potassium jarosite synthesized in this study. Based on their results and the results from natural samples analyzed in this study, it is probable that many natural jarosite samples are close to full Fe occupancy of the B site and are more closely correlated with the results of this study than previous structural studies done on synthetic non-stoichiometric samples.

Short-wave infrared (SWIR)

The short-wave infrared (SWIR) spectra, shown in Figure 11, are typical of the jarosite structure and the transmittance bands have been assigned based on the assignments by Bishop and Murad (2005). As can be seen from the spectra there is subtle difference between end-members hydronium jarosite and potassium jarosite that can be tracked across the solid-solution series. Specific bands could not be attributed to hydronium specifically but it can be seen that detail is lost from the spectra with increasing hydronium content. Specifically, bands that are dampened or lost are shoulders B (1514 nm), E (2214 nm), G (2296 nm), and area H (2380–2500 nm). Detailed assignments of the absorption bands are given in Figure 11. Velasco et al. (2005) found similar results from SWIR spectra collected on natural hydronium jarosite from San Miguel mine, SW Spain. Swayze et al. (2006) noted that OH-related vibrational absorptions became narrow and better defined in high temperature synthetic jarosite and alunite samples, which are fully hydroxylated. They postulated that replacement by H_2O of the hydroxyl groups in low-temperature samples due to an B site deficiency, disrupts strong vibrational coupling, weakening the spectral absorptions. As it is probable that there is protonation of OH^- groups in hydronium jarosite due to an A site deficiency, their model may also apply to our results. As there is a difference between spectra for hydronium-rich jarosite and potassium-rich jarosite, SWIR spectroscopy could be a useful field based method in determining a rough estimate of the hydronium content of the jarosite. As discussed in Fernández-Remolar et al. (2005), jarosite formation at Rio Tinto is probably similar to jarosite formation on Mars. Therefore, SWIR spectroscopy may be a useful method in determining the hydronium content of the Martian jarosites.

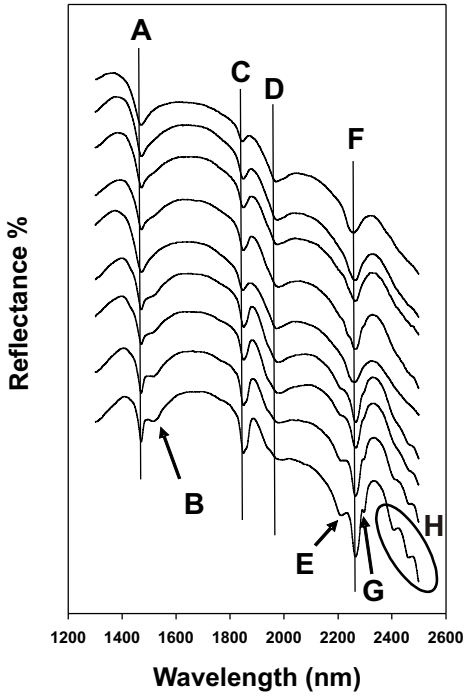

FIGURE 11. Short-wave infrared (SWIR) spectra of the hydronium–potassium jarosite solid-solution series. End-member hydronium jarosite is at the top, potassium jarosite is at the bottom, with intermediate stages of the solid-solution series in between. The bands have been assigned to the following: A-OH vibration and H_2O absorption, B-Fe-OH vibration, C-Fe-OH vibration, D-H_2O absorption, E-Fe-OH vibration, F-Fe-OH vibration, G-Fe-OH vibration, and H-$(SO_4)_2$ stretching and OH vibration. Band assignments were taken from Bishop and Murad (2005). Spectra have been offset for comparison.

ACKNOWLEDGMENTS

The authors thank Queen's University Analytical Services Unit for help chemically analyzing the samples. We thank Gregg Swazye, an anonymous reviewer, and Associate Editor George Lager for their valuable comments on the manuscript. The research was funded by an NSERC Discovery Grant to R.C.P.

REFERENCES CITED

Balzar, D. (1999) Voigt-function model in diffraction line-broadening analysis. International Union of Crystallography Monographs on Crystallography, 10, 94–126.

Baur, W.H. (1972) Prediction of hydrogen bonds and hydrogen atom positions in crystalline solids. Acta Crystallographica, B28, 1456–1465.

Begemann, M.H. and Saykally, R.J. (1985) A study of the structure and dynamics of the hydronium ion by high-resolution infrared laser spectroscopy. 1. The ν_3 band of $H_3{}^{16}O^+$. Journal of Chemical Physics, 82(8), 3570–3579.

Bishop, J.L. and Murad, E. (2005) The visible and infrared spectral properties of jarosite and alunite. American Mineralogist, 90, 1100–1107.

Brophy, G.P. and Sheridan, M.F. (1965) Sulfate studies IV: The jarosite–natrojarosite–hydronium jarosite solid-solution series. American Mineralogist, 50, 1595–1607.

Brown, J.B. (1970) A chemical study of some synthetic potassium–hydronium jarosites. Canadian Mineralogist, 10, 696–703.

Burns, R.G. (1987) Ferric sulfates on Mars. Journal of Geophysical Research, 92, E570–E574.

——— (1988) Gossans on Mars, p. 713–721. Proceedings of the 18th LPSC. LPI, Houston, Texas.

Cheary, R.W. and Coelho, A.A. (1998) Axial divergence in a conventional X-ray powder diffractometer I. Theoretical foundations. Journal of Applied Crystallography, 31, 851–861.

Chiari, G. and Ferraris, G. (1982) The water molecule in crystalline hydrates studied by neutron diffraction. Acta Crystallographica, B38, 2331–2341.

Clark, R.N., Swayze, G.A., Livo, K.E., Kokaly, R.F., Sutley, S.J., Dalton, J.B., McDougal, R.R., and Gent, C.A. (2003) Imaging Spectroscopy: Earth and planetory remote sensing with the USGS Tetracorder and expert systems. Journal of Geophysical Research, 108 (E12), 5/1–5/44.

Coelho, A.A. (2004) TOPAS-Academic. Coelho Software, Brisbane, Australia, http://members.optusnet.com.au/~alancoelho.

Drouet, C. and Navrotsky, A. (2003) Synthesis, characterization, and thermochemistry of K-Na-H_3O jarosites. Geochimica et Cosmochimica Acta, 11, 2063–2076.

Drouet, C., Pass, K.L., Baron, D., Draucker, S., and Navrotsky, A. (2004) Thermochemistry of jarosite-alunite and natrojarosite-natroalunite solid solutions. Geochimica et Cosmochimica Acta, 68, 2197–2205.

Dutrizac, J.E. (1983) Factors affecting alkali jarosite precipitation. Metallurgical Transactions, 14B, 531–539.

Dutrizac, J.E. and Jambor, J.L. (2000) Jarosites and their application in hydrometallurgy. In C.N. Alpers, J.L. Jambor, and D.K. Nordstrom, Eds., Sulfate Minerals, 40, p. 405–452. Reviews in Mineralogy and Geochemistry, Mineralogical Society of America, Chantilly, Virginia.

Dutrizac, J.E. and Kaiman, S. (1976) Synthesis and properties of jarosite-type compounds. Canadian Mineralogist, 14, 151–158.

Fernández-Remolar, D.C., Morris, R.V., Gruener, J.E., Amils, R., and Knoll, A.H. (2005) The Rio Tinto Basin, Spain: mineralogy, sedimentary geobiology, and implications for interpretation of outcrop rocks at Meridiani Planum, Mars. Earth and Planetary Science Letters, 240, 149–167.

Frost, R.L., Wills, R., Matt, M.L., Musumeci, A.W., and Martens, W. (2005) Thermal decomposition of natural and synthetic plumbojarosites: Importance in "archeochemistry." Thermochimica Acta, 432, 30–35.

García García, G. (1996) The Rio Tinto Mines Huelva, Spain. The Mineralogical Record, 27, 275–285.

Grohol, D., Nocera, D.G., and Papoutsakis, D. (2003) Magnetism of pure iron jarosites. Physical Review B: Condensed Matter and Materials Physics, 67, 064401/1–064401/13.

Hendricks, S.B. (1937) The crystal structure of alunite and the jarosites. American Mineralogist, 22, 773–784.

Hill, R.J. and Flack, H.D. (1987) The use of the Durbin-Watson *d* statistic in Rietveld analysis. Journal of Applied Crystallography, 20, 356–361.

Hölzer, G., Fritsch, M., Deutsch, M., Härtwig, J., and Förster, E. (1997) $K\alpha_{1,2}$ and $K\beta_{1,3}$ X-ray emission lines of the 3^d transition metals. Physical Review A, 56, 4554–4568.

Hudson-Edwards, K.A., Schell, C., and Macklin, M.G. (1999) Mineralogy and geochemistry of alluvium contaminated by metal mining in the Rio Tinto area, southwest Spain. Applied Geochemistry, 14, 1015–1030.

Kato, T. and Miuri, Y. (1977) The crystal structures of jarosite and svanbergite. Mineralogical Journal, 8, 419–430.

King, T.V.V., Clark, R.N., Ager, C., and Swayze, G.A. (1995) Remote mineral mapping using AVIRIS data at Summitville, Colorado and the adjacent San Juan Mountains. In H.H. Posey, J.A. Pendelton, and D. Van Zyl, Eds., Proceedings: Summitville Forum '95, 38, p. 59–63. Colorado Geological Survey Special Publication, Denver.

Klingelhöfer, G., Morris, R.V., Bernhardt, B., Schroder, C., Rodionov, D., de Souza, P.A.J., Yen, A.S., Gellert, R., Evlanov, E.N., Zubkov, B., Foh, J., Bonnes, U., Kankeleit, E., Gutlich, P., Ming, D.W., Renz, F., Wdowiak, T.J., Squyres, S.W., and Arvidson, R.E. (2004) Jarosite and hematite at Meridiani Planum from Opportunity's Mossbauer spectrometer. Science, 306, 1740–1745.

Kruse, F.A., Hauff, P.L., Dietz, J., Brock, J.C., and Hampton, L. (1989) Characterization and Mapping of Mine Waste at Leadville, Colorado, p. 79. Center of the Study of Earth from Space, University of Colorado, Boulder.

Kubisz, J. (1970) Studies on synthetic alkali-hydronium jarosites. I. Synthesis of jarosite and natrojarosite. Mineralogia Polonica, 1, 47–57.

Majzlan, J., Stevens, R., Boerio-Goates, J., Woodfield, B.F., Navrotsky, A., Burns, P.C., Crawford, M.K., and Amos, T.G. (2004) Thermodynamic properties, low-temperature heat-capacity anomalies, and single-crystal X-ray refinement of hydronium jarosite, $(H_3O)Fe_3(SO_4)_2(OH)_6$. Physics and Chemistry of Minerals, 31, 518–531.

Papike, J.J., Karner, J.M., Spilde, M.N., and Shearer, C.K. (2006) Terrestrial analogs of martian sulfates: Major and minor element systematics of alunite-jarosite from Goldfield, Nevada. American Mineralogist, 91, 1197–1200.

Ripmeester, J.A., Ratcliff, C.I., Dutrizac, J.E., and Jambor, J.L. (1986) Hydronium ion in the alunite-jarosite group. Canadian Mineralogist, 24, 435–447.

Rudolph, W.W., Mason, R., and Schmidt, P. (2003) Synthetic alunites of the potassium-oxonium solid-solution series and some other members of the group: synthesis, thermal and X-ray characterization. European Journal of Mineralogy, 15, 913–924.

Scott, K.M. (1987) Solid solution in, and classification of, gossan-derived members of the alunite-jarosite family, northwest Queensland, Australia. American Mineralogist, 72, 178–187.

Stoffregen, R.E. (1993) Stability relations of jarosite and natrojarosite at 150–250 °C. Geochimica et Cosmochimica Acta, 57, 2417–2429.

Stoffregen, R.E. and Alpers, C.N. (1987) Woodhouseite and svanbergite in hydrothermal ore deposits: Products of apatite destruction during advanced argillic alteration. Canadian Mineralogist, 25, 201–211.

Swayze, G.A., Smith, K.S., Clark, R.N., Sutley, S.J., Pearson, R.M., Vance, J.S., Hageman, P.L., Briggs, P.H., Meier, A.L., Singleton, M.J., and Rioth, S. (2000) Using imaging spectroscopy to map acidic mine waste. Environmental Science and Technology, 34, 47–54.

Swayze, G.A., Desborough, G.A., Clark, R.N., Rye, R.O., Stoffregen, R.E., Smith, K.S., and Lowers, H.A. (2006) Detection of jarosite and alunite with hyperspectral imaging: prospects for determining their origin on Mars using orbital sensors. Workshop on Martian Sulfates as Recorders of Atmospheric-Fluid-Rock Interactions, Houston, Texas, 2006, http://www.lpi.usra.edu/meetings/sulfates2006/pdf/7072.pdf.

Velasco, F., Alvaro, A., Suarez, S., Herrero, J.-M., and Yusta, I. (2005) Mapping Fe-bearing hydrated sulphate minerals with short wave infrared (SWIR) spectral analysis at San Miguel mine environment, Iberian Pyrite Belt (SW Spain). Journal of Geochemical Exploration, 87, 45–72.

Wills, A.S. and Harrison, A.H. (1996) Structure and magnetism of hydronium jarosite, a model Kagome antiferromagnet. Journal of the Chemical Society-Faraday Transactions, 92, 2161–2166.

Young, R.A. (1993) Introduction to the Rietveld method. In R.A. Young, Ed., The Rietveld Method, p. 1–38. Oxford University Press, U.K.

MANUSCRIPT RECEIVED AUGUST 24, 2006
MANUSCRIPT ACCEPTED APRIL 16, 2007
MANUSCRIPT HANDLED BY GEORGE LAGER